Flatness-Based Feedback Control of an Automotive Solenoid Valve

Soon K. Chung, Charles Robert Koch, *Member, IEEE,* Alan F. Lynch, *Member, IEEE*

***Abstract*— This paper considers the control of solenoid valve actuators used for gas exchange in internal combustion engines. Although solenoid valves offer performance benefits over traditional camshaft-based valve systems, maintaining low impact velocity is a critical performance requirement. Flatness provides a convenient framework for meeting a number of performance specifications on the valve's end motion. The proposed control design incorporates voltage constraints, nonlinear magnetic effects, and various motion planning requirements. A flat output acts as a design parameter and is parameterized with a spline basis. A nonlinear feasibility problem is solved to obtain optimal spline coefficients such that performance requirements are met. The resulting flat output provides an open-loop control which is augmented with feedback so that a linear stable tracking error system results. The proposed control scheme is demonstrated in simulation and on an experimental testbed. The performance of a Proportional-Integral controller is compared experimentally to the flatness-based method.**

***Index Terms*— Digital control, internal combustion engines, modeling, motion-planning, nonlinear systems, solenoids, tracking.**

I. Introduction

SIGNIFICANT improvement in spark ignition internal combustion (IC) engine fuel consumption and reduction of hazardous exhaust emissions can be obtained with solenoid valve actuators to control engine gas exchange valves. These performance benefits over conventional camshaft engines result from being able to adjust individual valve timing over the entire load-speed range [33]. Novel combustion techniques such as Homogeneous Charge Compression Ignition (HCCI) [2], [12], which also potentially reduce fuel consumption and exhaust pollutants, can be used with variable valve timing [7] to adjust in-cylinder conditions during engine transients. A number of variable valve timing designs exist including solenoid valves [32] or hydraulic system [1] based solutions.

Two important criteria must be met when solenoids are used to actuate gas exchange valves in an IC engine. First, the transition time for a valve to open/close should take approximately 4 ms in order to meet maximum engine speeds of 5000 – 6000 RPM [31]. Second, impact velocities of less than 0.1 m/s are desirable for maintaining acceptable engine acoustical noise levels, and ensuring valve seatings and wear requirements are met [38]. However, performing efficient solenoid valve control is a challenging problem due in part to an actuator's uncertain nonlinear behaviour. This complex behaviour results from eddy currents, magnetic saturation, limited range of authority, and sensitivity to parameter variation and load disturbances. Existing control work often applies linear position and velocity feedback in an effort to limit valve impact velocities [23]. Other proposed solutions include an energy-based method [35] and a nonlinear scheme using acoustical measurements where the controller is tuned based on sound pressure intensity [31]. A sensorless approach suggested in [4], [5] alleviates the need for position and velocity measurements. Here each coil is used for both current measurement and force generation. For most of these strategies, a combination of open and closed-loop control is performed [17]. After the valve is released, open-loop compensation is enabled during the middle stages of motion. A feedback scheme (called end-control here) then follows in the final portion of the valve motion to ensure the valve lands at a desired velocity. The objective of open-loop control is to setup valve motion conditions so that when the end-control is switched on, low valve impact is achievable. This strategy is necessary due to the system's limited control authority at large air gaps.

This paper exploits a flatness property of the solenoid valve actuator model [15], [16]. Flatness is particularly well-suited for designing a feasible open-loop trajectory which respects a number of competing performance requirements. As well, it naturally leads to a feedback control which can account for model error and disturbances. The proposed flatness-based control is intended for the final stage of armature motion, and we do not consider the initial control phase. In addition to an open-loop trajectory design which incorporates motion planning constraints as in [21], [22], the proposed method also accounts for magnetic saturation. A nonlinear feasibility problem is solved numerically to compute a desired open-loop trajectory which meets performance requirements. Optimization applied to motion planning has been well-studied in [3], [13], [28], [29], [30] and [37]. For the class of flat systems, the optimization problem is simplified by eliminating dynamic constraints. This is because system variables can be differentially parameterized by a flat output which acts as the design parameter in the optimization problem.

This paper is organized as follows. Section II presents a model of the solenoid valve actuator which includes magnetic saturation. Section III derives a flatness-based feedback end-control. Section IV outlines the open-loop trajectory design. Section V demonstrates the method in simulation, and Section VI validates the control scheme experimentally.

Manuscript received August 26, 2005; revised June 6, 2006. This work was supported in part by the Natural Sciences and Engineering Research Council of Canada.

S.K. Chung and C.R. Koch are with the Department of Mechanical Engineering, University of Alberta. A.F. Lynch is with the Department of Electrical and Computer Engineering, University of Alberta.

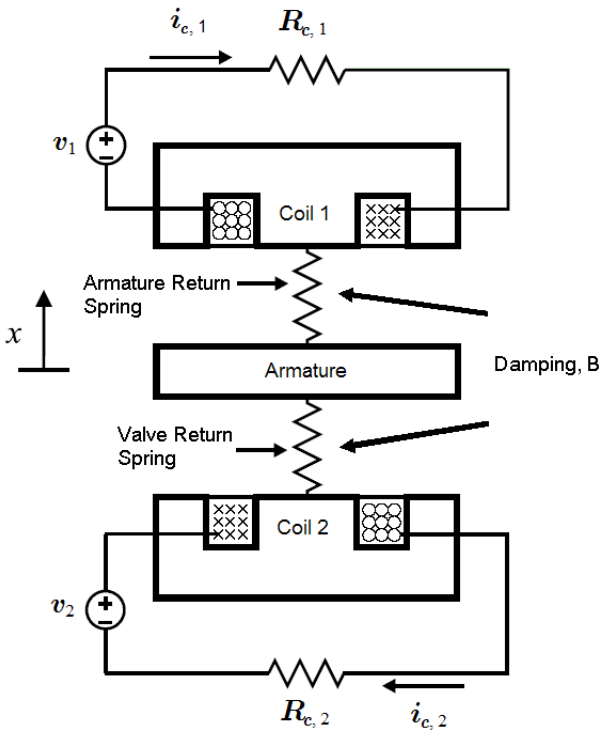

Fig. 1. Schematic of a two-spring solenoid actuator valve. Here x is the valve position, $i_{c,i}$ is coil current, $R_{c,i}$ is the coil resistance and v_i is the coil voltage where $i = 1$ denotes the closer and $i = 2$ denotes the opener coil.

II. Modeling

The solenoid valve actuator considered here is similar to that proposed in [32]. This linear actuator, shown schematically in Figure 1, consists of two opposing electromagnets that move an armature-valve assembly. The device is spring-loaded to store mechanical energy with an unforced rest position midway between the coils. Experimental data from a prototype valve for a modern spark ignition engine provided by Daimler-Chrysler is used for identifying simulation model parameters. The armature position, denoted by x, varies on $[-4, 4]$ mm with $x = 0$ being the midpoint between coils as shown in Figure 1. Using a flux saturation model similar to [19], we take

$$\lambda(x, i_c) = \lambda_s(1 - e^{-i_c f(x)}), \quad i_c \geq 0 \tag{1}$$

where λ is coil flux linkage, λ_s is saturated coil flux linkage, i_c is coil current and f is defined as

$$f(x) = \frac{2\,C_1}{C_2 - x} + C_3$$

This form of f was chosen such that the flux linkage model (1) is consistent with previous work [21] for small i_c; this gives a physical interpretation for C_i. Only Coil 1 is turned on and we assume no magnetic coupling between coils. This is a valid assumption since both coils are not energized at the same time. The force F exerted by Coil 1 on the armature is obtained by differentiating the coenergy:

$$W_c(x, i_c) = \int_0^{i_c} \lambda(x, \xi) d\xi$$

Magnetic force is given by

$$F(x, i_c) = \frac{\partial W_c}{\partial x}(x, i_c) \tag{2}$$

Substituting (1) into (2) gives

$$F(x, i_c) = \frac{\lambda_s f'(x)}{f^2(x)} \left[1 - (1 + i_c f(x))\, e^{-i_c f(x)}\right] \tag{3}$$

where $f'(x) = 2C_1/(C_2 - x)^2$. Coefficients λ_s, C_1, C_2 and C_3 are determined by taking a least squares fit to static experimental force data. The resulting parameters are $\lambda_s = 0.0763$ Wb, $C_1 = 2.30 \cdot 10^{-2}$ mm/A, $C_2 = 4.04$ mm and $C_3 = 4.18 \cdot 10^{-4}\text{A}^{-1}$. Using these parameters in (3), the magnetic force expression has a good fit with experimental data, see Figure 2. Newton's law for the armature gives

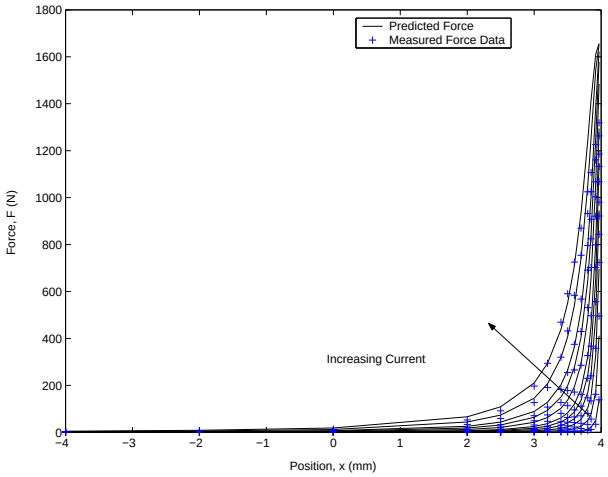

Fig. 2. Comparison of (3) with experimental data – $i_c \in \{1, 2, 4, 6, 8, 10, 15, 20, 25, 30, 35\}$ A.

$$m\ddot{x} = F(x, i_c) + \mathcal{A}(x, \dot{x}) \tag{4}$$

where $\mathcal{A}(x, \dot{x}) = -(k_s x + B\dot{x})$, $k_s x$ is the spring force, $B\dot{x}$ is the viscous friction and m is the moving mass. The end-control method proposed here actuates only one coil since air gap distances, as shown in Figure 2, would be too large for the other coil to exert any substantial force when the armature is near the activated coil. We ignore disturbance load forces acting on the valve.

The parameters of the mechanical subsystem are obtained by system identification. Armature position for free oscillations are experimentally measured and Matlab's Prediction Error method `PEM` in the System Identification Toolbox [25], [26] is used to obtain estimates of m, K_s and B in (4). The results are $m = 0.2773$ kg, $k_s = 250.98$ N/mm and $B = 12.75$ Ns/m.

The coil dynamics can be approximately represented by

$$\frac{d\lambda}{dt}(x, i_c) = v - R_c i_c \tag{5}$$

where v is coil input voltage and R_c is coil resistance. The value of $R_c = 0.52\ \Omega$ is measured directly. Solving for the

time derivative of i_c in (5) gives

$$\frac{di_c}{dt} = \frac{1}{\frac{d\lambda}{dt}(x,i_c)}\left(v - R_c i_c - \frac{d\lambda}{dx}(x,i_c)\frac{dx}{dt}\right) \quad (6)$$
$$= \frac{e^{i_c f(x)}}{\lambda_s f(x)}\left(v - R_c i_c - \lambda_s f'(x)\ \dot{x}\ i_c\ e^{-i_c f(x)}\right)$$

The system has three states: armature position x, armature velocity $\dot{x}$ and coil current i_c. The coil voltage v is the system input.

III. Flatness-based End-Control

A flatness-based static state feedback control is derived so that the armature position converges exponentially to a desired trajectory. As in [24], [27] and [39] differential flatness provides a convenient framework for solving this trajectory tracking problem. A flat output is defined as

$$y = x \quad (7)$$

Using (4) and (7), it can be shown that the states can be expressed as functions of y and a finite number of its time derivatives:

$$x = y \quad (8a)$$
$$\dot{x} = \dot{y} \quad (8b)$$
$$i_c = -\frac{1}{f(y)}\left[W_{-1}(-g(y,\ \dot{y},\ \ddot{y})/e) + 1\right] \quad (8c)$$

where

$$g(y,\ \dot{y},\ \ddot{y}) = 1 - \frac{f^2(y)[m\ddot{y} - \mathcal{A}(y,\dot{y})]}{\lambda_s f'(y)} \quad (8d)$$

and W_{-1} is a real-valued branch of Lambert's W function [10]. The Lambert W function $W(z)$ is defined such that for every complex number z, $z = W(z)e^{W(z)}$. Since $0 \le g(y,\ \dot{y},\ \ddot{y}) < 1$, the argument of W_{-1} is between $-1/e$ and 0, and this ensures that W_{-1} is well-defined.

The third time derivative of y is used to obtain an expression for voltage input

$$y^{(3)} = \frac{1}{m}\left[\dot{F}(y,i_c) + \dot{\mathcal{A}}(y,\ \dot{y})\right] \quad (9)$$

with

$$\dot{F}(y,i_c) = 2\dot{y}F(y,i_c)\left[\frac{1}{C_2 - y} - \frac{f'(y)}{f(y)}\right] + \frac{i_c f'(y)}{f(y)}[v - R_c i_c] \quad (10)$$

Solving for v gives

$$v = \frac{f(y)}{i_c f'(y)}\left[m y^{(3)} - \dot{\mathcal{A}}(y,\ \dot{y}) - 2\dot{y}F(y,i_c)\left[\frac{1}{C_2 - y} - \frac{f'(y)}{f(y)}\right]\right] + R_c i_c \quad (11)$$

Equation (11) has a singularity at $i_c = 0$, however, the motion planning described in Section IV ensures nonzero open-loop current to avoid this condition. From (8) and (11) the system is differentially flat, i.e., we can express state and input as a function of y and a finite number its time derivatives. Consequently, convenient methods for solving trajectory tracking problems exist.

Although the flatness-based strategy solves the open-loop trajectory tracking problem, an additional feedback is required to compensate for initial condition output tracking error, external disturbances, and parameter variations. Denote y_d as the desired trajectory for the armature and $\tilde{y} = y - y_d$ as the tracking error. In order to obtain a closed-loop voltage which achieves linear error dynamics

$$\tilde{y}^{(3)} + k_2\ddot{\tilde{y}} + k_1\dot{\tilde{y}} + k_0\tilde{y} = 0. \quad (12)$$

we solve (12) for $y^{(3)}$ to obtain

$$y^{(3)} = y_d^{(3)} - k_2\ddot{\tilde{y}} - k_1\dot{\tilde{y}} - k_0\tilde{y} \quad (13)$$

Substituting this expression for $y^{(3)}$ into (11) gives the expression for the closed-loop static state feedback voltage:

$$v = \frac{f(y)}{i_c f'(y)}\left[m[y_d^{(3)} - k_2\ddot{\tilde{y}} - k_1\dot{\tilde{y}} - k_0\tilde{y}] - \dot{\mathcal{A}}(y,\ \dot{y}) - 2\dot{y}F(y,i_c)\left[\frac{1}{C_2 - y} - \frac{f'(y)}{f(y)}\right]\right] + R_c i_c \quad (14)$$

We choose k_0, k_1 and k_2 to ensure y converges to y_d exponentially. The robustness of this control law to model error is discussed in Appendix I.

IV. Open-Loop Trajectory Design

In this section we describe the design of a suitable desired trajectory y_d to meet the system performance specifications. We constrain the initial and final armature positions as

$$y_d(t_0) = 2.55 \text{ mm} \quad (15)$$
$$y_d(t_f) = 4 \text{ mm} \quad (16)$$

where t_0 is the time at which the end-control is activated and t_f is the time at which the armature lands. The constraints on velocity are

$$\dot{y}_d(t_0) = 2.59 \text{ m/s} \quad (17)$$
$$\dot{y}_d(t_f) \le 0.1 \text{ m/s} \quad (18)$$
$$\dot{y}_d(t) \ge 0, \quad t_0 < t < t_f \quad (19)$$

Constraint (18) is critical in ensuring reduced wear and acoustical noise as discussed in Section I. The constraints on acceleration and current are

$$\ddot{y}_d(t_0) = \left[F(y_d(t_0), i_c(t_0)) + \mathcal{A}(y_d(t_0), \dot{y}_d(t_0))\right]/m \quad (20)$$
$$\ddot{y}_d(t_f) = 0 \quad (21)$$
$$\ddot{y}_d(t) > \mathcal{A}(y_d(t), \dot{y}_d(t))/m \quad (22)$$
$$i_c(t_0) = 8.9 \text{ A} \quad (23)$$

Since only one coil is being used, constraint (22) is required to ensure only attractive forces are applied. We expect the initial open-loop control phase ensures armature conditions are close to the prescribed desired initial values for the position, velocity, and current in (15), (17), and (23) respectively. These limits were chosen based on experimental testing.

Using (11) we can impose a constraint on the maximum voltage during end-control:

$$|v(t)| \leq 42 \text{ V}, \quad t_0 \leq t \leq t_f \tag{24}$$

The value of 42 V is chosen to match the experimental actuator design requirements and possible future on-board vehicle voltage standards [6].

Following [27], we parameterize y_d using a B-spline basis:

$$y_d(t) = \theta^T B(t) \quad t_0 \leq t \leq t_f \tag{25}$$

where θ is a vector of spline coefficients and B is a vector of B-spline basis functions of order k defined on the interval $[t_0, t_f]$. Due to (11), we take fourth order (i.e., quartic or $k = 5$) B-splines with 6 evenly spaced simple knots on $[t_0, t_f]$ to ensure $y_d^{(3)}$ is well-defined and we can evaluate (14). The nonlinear feasibility problem is solved using Matlab's Spline and Optimization Toolboxes. Conditions (15), (16), (17), (20) and (21) are linear equality constraints. Conditions (18) and (19) are linear inequality constraints. Condition (22) is discretized in time and becomes a nonlinear inequality constraints. Choosing $t_0 = 0$ and $t_f = 1.84$ ms, the optimization algorithm converges to a feasible trajectory shown in Figures 6.

V. Simulation

Due to limited coil force at large airgaps, closed-loop control (14) is applied in the final stage of motion [38], [31]. That is, end-control is performed only in the last 1.45 mm of the entire 8 mm motion. We take actual system conditions of $x(t_0)$ = 2.53 mm and $\dot{x}(t_0)$ = 2.58 m/s. These values differ from the initial conditions of the trajectory design defined in Section IV to investigate sensitivity to initial condition error. A block diagram of the control strategy for closer coil is shown in Figure 3 – the control strategy for the opener coil is similar and both coils are never switched on at the same time. Controller gains for the error dynamics are selected to ensure the simulation converges to the designed trajectory within the time interval $t_f - t_0 = 1.84$ ms. The values for the gains are $k_0 = 8.0 \cdot 10^{12}$ s^{-3}, $k_1 = 1.02248 \cdot 10^9$ s^{-2} and $k_2 = 6 \cdot 10^4$ s^{-1}.

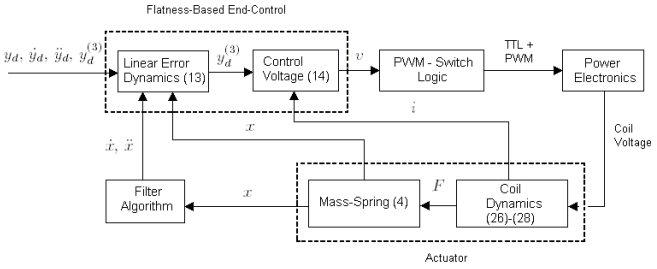

Fig. 3. Scheme of flatness-based voltage end-control with estimation of state variables.

The simulation assumes linear voltage v can be applied to the coil using a switch logic block to output PWM signals into the power electronics. A power electronics model that drives the coil through on-off switching in the H-bridge is included to improve simulation accuracy of coil voltage transients [8]. Filter algorithms which are needed in the experiment are also implemented in the simulation model to estimate armature velocity and acceleration [9]. A constant gain Kalman filter is used to estimate the velocity, and the acceleration is estimated using a exponentially weighted moving average of velocity. Since predictions of current dynamics are needed for determining electromagnetic forces accurately, eddy current effects are also considered in the simulation to provide a more accurate model of the real actuator. Eddy currents are induced as a direct result of flux changes within the actuator coil [14], [18]. For fast operation, eddy current losses can substantially affect actuator performance due to net flux reductions that cause electromechanical response times to increase. However, computing exact amplitude and distribution of eddy currents is a challenging problem that depends on the nature of time-varying current flow in the coil and the position of the armature [36]. A useful model for approximating eddy currents is an equivalent circuit representation consisting of a secondary-branch resistance R_e and an inductance L_e [34], [8]. This model is

$$\frac{d\lambda}{dt}(x, i_c) = v - R_c[i_c + i_e] \tag{26}$$

$$i = i_c + i_e \tag{27}$$

$$\frac{di_e}{dt} = \frac{1}{L_e(x, i_c)}\Big[v - R_c[i_c + i_e] - R_e(x, i_c) i_e\Big] \tag{28}$$

where $R_e(x, i_c)$ is a parasitic resistance, $L_e(x, i_c)$ is a parasitic inductance and i_e is an eddy current. Figure 4 shows the circuit diagram for (26)–(28); it is a more complex coil model than that used for control design. The functions $R_e(x, i_c)$ and $L_e(x, i_c)$ in (28) are difficult to determine analytically, but using transient FEA solutions and least squares optimization, look-up tables for these functions can be obtained.

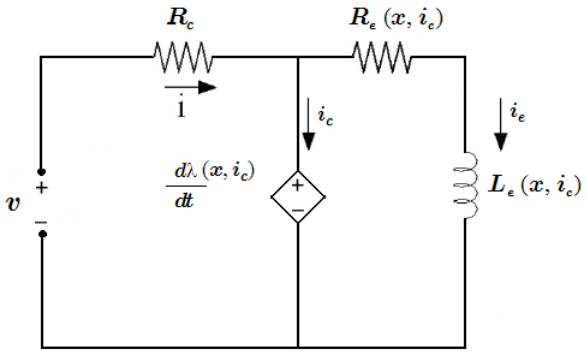

Fig. 4. Equivalent circuit diagram with augmented eddy current model.

VI. Experimental Setup

The experimental setup is shown in Figure 5. A real-time implementation of the control law is coded in C, and a dSPACE DS1103 control board reads current and armature position as analog inputs. PWM and digital TTL signals

to the power electronics are output at a sample rate of 50 kHz. The H-bridge power electronics provide three output modes ($+42$ V, 0 V, and -42 V) for regulating voltage to the actuator coils [9]. All modes are achieved by switching two high speed voltage-controlled power IGBT transistors. One transistor is switched at 50 kHz while the other receives a PWM signal with a 50 kHz duty cycle. If switching frequencies are sufficiently high it is reasonable to assume that PWM duty cycle approximates linear average voltage [11], [31]. The DC power supply is a Sorenson DCS60-18E 1kW switching power supply set to 42 VDC. Current measurements are conducted with a Hall-effect (LEM LA55-P) current sensor. Armature displacement measurements are measured by an eddy current position sensor. Since the testbed does not have a hydraulic lash adjuster, the exhaust/intake valve can be assumed to be rigidly connected to the armature without separation throughout the entire range of motion.

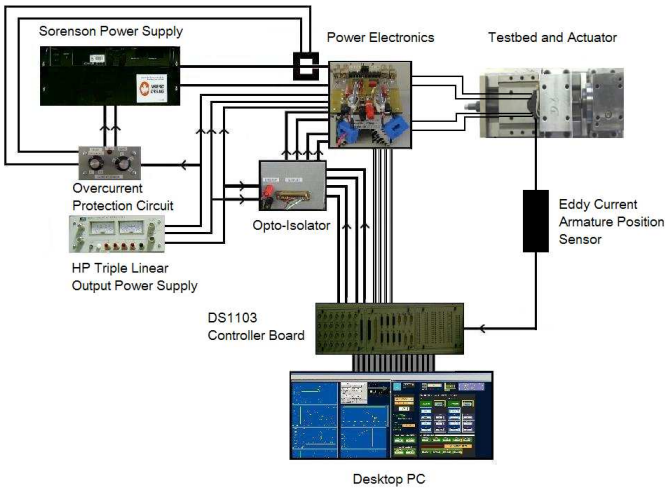

Fig. 5. Schematic of experimental testbench showing the dSpace controller, the solenoid actuator, power electronics and DC Power.

VII. Experimental Results

Both a flatness-based and Proportional-Integral (PI) controller are experimentally implemented. The PI current feedback controller

$$i_{pi} = K_p \tilde{y} + K_I \int_0^t \tilde{y}(\tau) d\tau$$

uses $\tilde{y}$ to generate a coil current. The gains K_p and K_I are tuned to obtain the best possible performance and this result is compared to the flatness-based control. Both feedback controllers require an initial open-loop current control to deliver the armature to a suitable suitable condition to initiate end-control. For the case of the flatness-based control, the armature is delivered to $x(t_0) = 2.525$ mm and $\dot{x}(t_0) = 2.580$ m/s. Note these conditions are close to the prescribed initial conditions used in the simulation described in Section V. For the PI controller, the armature is delivered to $x(t_0) = 2.309$ mm and $\dot{x}(t_0) = 2.690$ m/s. The PI controller has a proportional gain $K_p = 2500$ A/m and integral gain $K_I = 350$ A/m^2.

Figures 6–10 show experimental results obtained for both controllers. The simulation results for flatness-based control are also superimposed on the graphs. In Figure 6 the flatness-based control shows good convergence of armature position to its desired reference. The simulation results show good agreement with the experimental data. Discrepancies with simulation are more apparent in Figure 7 where the flatness-based control achieves an acceptable end-velocity of about 0.11 m/s. Figure 7 also illustrates slight impact bounce effects not observed in simulation. After-impact dynamics are not modeled in simulation since we are only interested in achieving low impact velocity at initial contact. Experimental results confirm that if the low impact velocity condition is satisfied, bounce dynamics can be neglected. Armature impact velocity under the PI controller is about 0.12 m/s. The higher impact velocity can be attributed to increased current levels as shown in Figure 9. Figure 8 and 9 show good agreement between actual and simulated acceleration and current results, respectively. Actual voltage levels are shown to be within ± 42 V in Figure 10. When $t \leq 2.85$ ms, +42 V is switched on to pull the armature in.

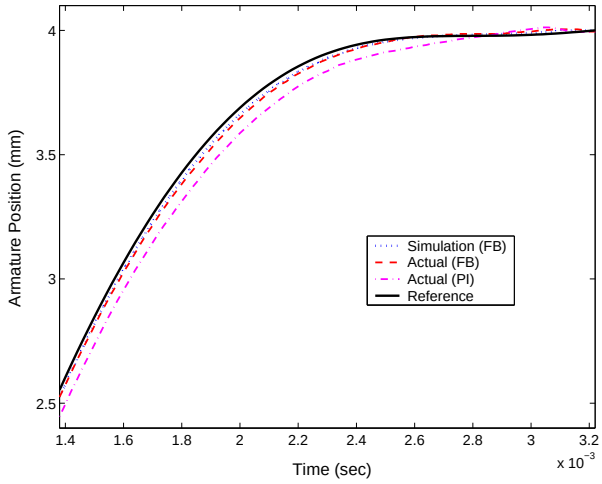

Fig. 6. Desired y_d, simulated and measured armature position x.

Fifty experimental closing tests are conducted using the flatness-based control in order to verify its ability to repeatedly maintain low impact velocity. Given a variation in the initial state at which the end-control was activated, the flatness-based design consistently landed the armature softly. An average velocity of 0.097 m/s with a standard deviation of 0.028 m/s is obtained as shown in Figure 11. A similar test cycle using the PI controller is performed. Figure 12 shows the distribution of armature impact velocities with a slightly higher average velocity of 0.12 m/s and standard deviation of 0.045 m/s. From these results we conclude that the flatness-based end-control provides robust performance as long as initial condition error is small. In addition, flatness-based control is enabled later in the valve motion than PI end-control, and judging by the input trajectories shown in Figures 9 and 10 seems to require less control effort.

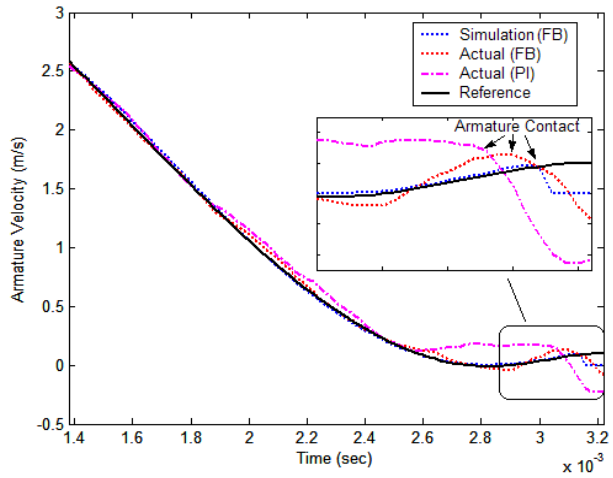

Fig. 7. Desired y_d, simulated and measured armature velocity $\dot{x}$.

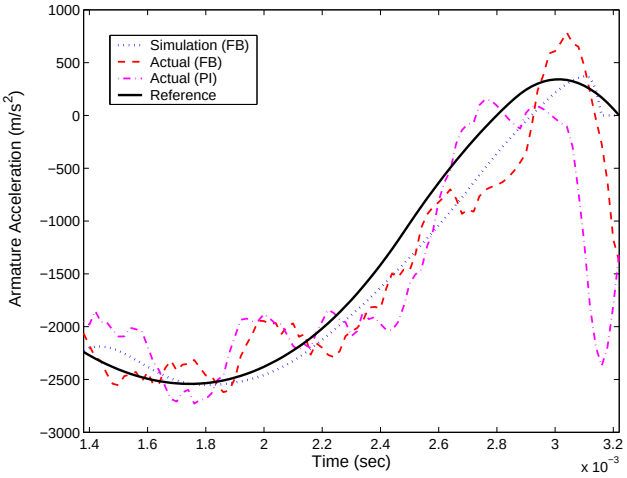

Fig. 8. Desired $\ddot{y}_d$, simulated and measured armature acceleration $\ddot{x}$.

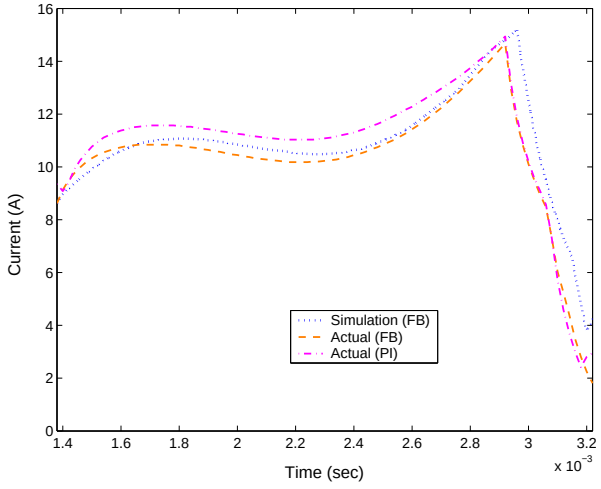

Fig. 9. Simulated and measured current i_c.

VIII. Conclusion

The combination of stringent performance requirements and complex nonlinear dynamics makes solenoid valve motion control a challenging problem. This paper presents a lumped parameter solenoid valve simulation model which includes magnetic saturation and eddy current effects. The parameters of the model are obtained from experimental data of a prototype actuator. This solenoid valve model accurately predicts the dynamics of the system when compared to experiment; hence, the simulation model is a useful tool for control algorithm validation. The proposed flatness-based control allows for an open-loop design which includes a number of important motion planning constraints. A flat output is parameterized using a spline basis, and a nonlinear feasibility problem is

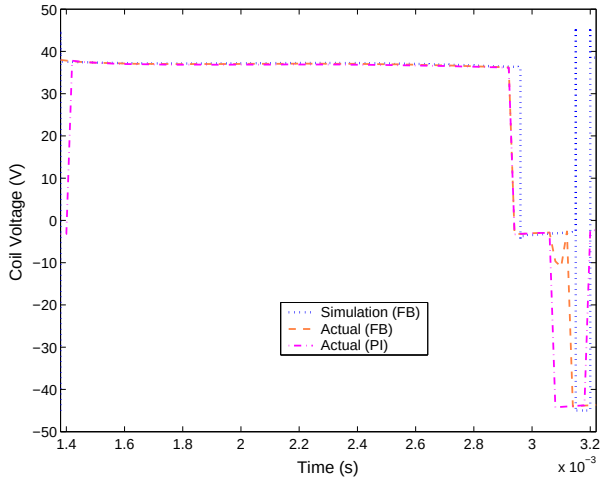

Fig. 10. Simulated and actual voltage v.

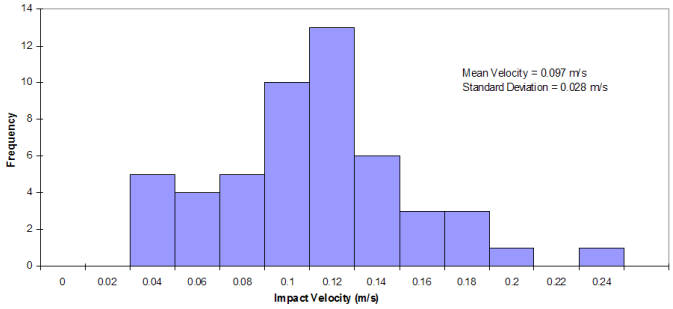

Fig. 11. Distribution of armature impact velocity for 50 cycles via flatness-based voltage end-control.

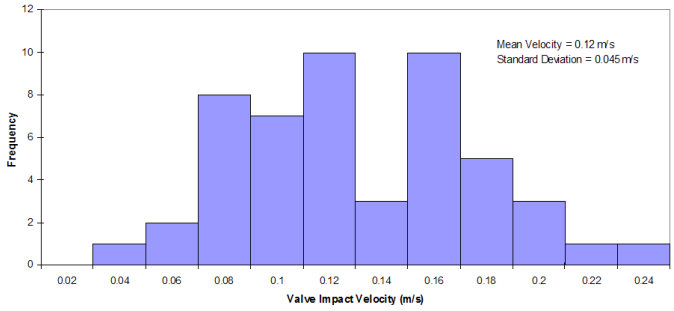

Fig. 12. Distribution of armature impact velocity for 50 cycles via Proportional-Integral current end-control.

solved numerically to obtain the suitable open-loop control. A PI controller is implemented in order to compare its performance with the flatness-based design. Consistent low impact performance is demonstrated for the proposed control. The PI control produced a slightly higher average velocity with a greater variation.

ACKNOWLEDGMENT

The authors wish to thank Daimler-Chrysler for the donation of the solenoid valve actuator and their technical assistance.

APPENDIX I
ROBUSTNESS OF FLATNESS-BASED CONTROL LAW

We recall the control law (11) and define the vectors $\tilde{z} = (\tilde{y}, \dot{\tilde{y}}, \ddot{\tilde{y}})^T$, $z = (y, \dot{y}, \ddot{y})^T$, and $z_d = (y_d, \dot{y}_d, \ddot{y}_d)^T$. We can renotate the control (14) as

$$v(\zeta, t) = \alpha(\zeta) - \beta(\zeta) K \tilde{z} \tag{29}$$

for appropriately defined functions α, β of the system state $\zeta = (x, \dot{x}, i_c)^T$ and $K = (k_0, k_1, k_2)$. We can rewrite the tracking error dynamics as

$$\dot{\tilde{z}} = A\tilde{z} + B\beta^{-1}(\zeta)(v - \alpha(\zeta)) \tag{30}$$

where (A, B) is in Brunovsky controller form. If we apply control (29) to this system we have LTI tracking error dynamics

$$\dot{\tilde{z}} = (A - BK)\tilde{z} \tag{31}$$

or equivalently (12). However, suppose we compute the control (14) based on an incorrect model assuming model structure is known, the resulting control is denoted

$$\hat{v}(\zeta, t) = \hat{\alpha}(\zeta) - \hat{\beta}(\zeta) K (\hat{z} - z_d) \tag{32}$$

where $\hat{\cdot}$ denotes a function based on an incorrect model. Substituting (32) into (30) gives the perturbed error dynamics

$$\dot{\tilde{z}} = (A - BK)\tilde{z} + B\delta(\tilde{z}, t) \tag{33}$$

where

$$\begin{aligned}\delta(z, t) = \beta^{-1}(\zeta)\big[&\hat{\alpha}(\zeta) - \alpha(\zeta) + (\beta(\zeta) - \hat{\beta}(\zeta))K\tilde{z} \\ &+ \hat{\beta}(\zeta)K(\tilde{z} - \hat{\tilde{z}})\big]_{\zeta = \zeta(z)}\end{aligned} \tag{34}$$

where $\hat{\tilde{z}} = \hat{z} - z_d$. Now we can apply a straightforward modification of [20, Lem. 13.3] which states that for a system (33) with $A - BK$ Hurwitz and $P > 0$, the solution to

$$P(A - BK) + (A - BK)^T P = -I$$

with $k \geq 0$ a constant less than $1/(2\,\|PB\|_2)$, then

- if $\|\delta(\tilde{z}, t)\| \leq k\,\|\tilde{z}\|, \forall \tilde{z}, t$, the origin of (33) is globally exponential stable,
- if $\|\delta(\tilde{z}, t)\| \leq k\,\|\tilde{z}\| + \epsilon, \forall \tilde{z}, t$, for some $\epsilon > 0$, the tracking error $\tilde{z}$ will be globally ultimately bounded by ϵc for some $c > 0$.

Local stability and ultimate bounded results are also immediate. Hence, provided the norm of the model error term δ can be linearly bounded, the proposed control will ensure stable tracking or ultimate boundedness.

REFERENCES

[1] J. Allen and D. Law, "Production electro-hydraulic variable valve-train for a new generation of I.C. engines," *SAE 2002-01-1109*, 2002.
[2] M. Atkins and C. Koch, "The effect of fuel octane and diluent on HCCI combustion," *Proc. IMechE*, vol. 219, part D, pp. 665–675, May 2005.
[3] A. J. Bryson and Y. Ho, *Applied Optimal Control*. New York, NY: Blaisdell Publishing Company, 1969.
[4] S. Butzmann, J. Melbert, and A. Koch, "Sensorless control of electromagnetic actuators for variable valve train," *SAE 2000-01-1225*, 2000.
[5] S. Butzmann and J. Melbert, "Method for controlling an electromechanical actuator," *US Patent 6,648,297*, Nov. 18, 2003.
[6] W. S. Chang, T. A. Parlikar, M. D. Seeman, D. J. Perreault, J. G. Kassakian, and T. A. Keim, "A new electromagnetic valve actuator," *IEEE Workshop Power Electron. Transp., Auburn Hills, MI*, pp. 109–118, Oct. 2002.
[7] R. Chladny, "Modeling and simulation of automotive gas exchange valve solenoid actuators," Master's thesis, Department of Mechanical Engineering, University of Alberta, 2003.
[8] R. Chladny, C. R. Koch, and A. F. Lynch, "Modeling of automotive gas exchange solenoid valve actuators," *IEEE Trans. on Magnetics*, vol. 41, no. 6, pp. 1–9, Mar. 2005.
[9] S. Chung, "Flatness-based end-control of a gas exchange solenoid actuator for IC engines," Master's thesis, Department of Mechanical Engineering, University of Alberta, 2005.
[10] R. Corless, G. Gonnet, D. Hare, D. Jeffrey, and D. Knuth, "On the Lambert W function," *Advances in Computational Mathematics*, vol. 5, pp. 329–359, 1996.
[11] F. Deng and T. W. Nehl, "Analytical modeling of eddy-current losses caused by pulse-width-modulation switching in permanent-magnet brushless direct-current motors," *IEEE Trans. on Magnetics*, vol. 34, no. 5, pp. 3728–3736, Sep. 1998.
[12] K. Epping, S. Aceves, R. Bechtold, and J. Dec, "The potential of HCCI combustion for high efficiency and low emissions," *SAE 2002-01-1923*, 2002.
[13] T. N. Faiz, "Real-time and optimal trajectory generation for nonlinear systems," Ph.D. dissertation, Department of Mechanical Engineering, University of Delaware, 1999.
[14] J. J. Feeley, "A simple dynamic model for eddy currents in a magnetic actuator," *IEEE Trans. on Magnetics*, vol. 32, no. 2, pp. 453–458, Mar. 1996.
[15] M. Fliess, J. Lévine, P. Martin, and P. Rouchon, "Flatness and defect of non-linear systems: Introductory theory and examples," *Int. J. Control*, vol. 61, no. 6, pp. 1327–1361, Jun. 1995.
[16] ——, "A Lie-Bäcklund approach to equivalence and flatness of nonlinear systems," *IEEE Trans. Auto. Contr.*, vol. 44, no. 5, pp. 922–937, May 1999.
[17] C. Gimselmann and J. Melbert, "Improved robustness and energy consumption for sensorless electromagnetic valve train," *SAE 2003-01-0030*, 2003.
[18] C. Hartwig, O. Josef, and K. Gebauer, "Transients of electromagnetic valve train (EMVT) actuators," *SAE 2004-01-1338*, 2004.
[19] M. Ilic'-Spong, R. Marino, S. Peresada, and D. Taylor, "Feedback linearizing control of switched reluctance motors," *IEEE Trans. Auto. Contr.*, vol. 32, no. 5, pp. 371–379, May 1987.
[20] H. K. Khalil, *Nonlinear Systems*, 3rd ed. Englewood Cliffs, NJ: Prentice-Hall, 2002.
[21] C. Koch, A. Lynch, and R. Chladny, "Modeling and control of solenoid valves for internal combustion engines," *Proc. 2nd IFAC Mech. Sys, Berkeley, CA*, pp. 213–218, 2002.
[22] C. Koch, A. Lynch, and S. Chung, "Flatness-based automotive solenoid valve control," *Proc. 6th IFAC-Symposium NOLCOS, 2004*, vol. 3, pp. 1091–1096.
[23] R. Konrad, "Verfahren zur Bewegungssteuerung für einen Anker eines elektromagnetischen Aktuators," *German Patent Appl. 19834548*, Jul. 31, 1998.
[24] J. Lévine, J. Lottin, and J.-C. Ponsart, "A nonlinear approach to the control of magnetic bearings," *IEEE Trans. Contr. Syst. Technol.*, vol. 4, no. 5, pp. 524–544, Sep. 1996.
[25] L. Ljung, *System Identification: Theory for the User*. Englewood Cliffs, NJ: Prentice-Hall, 1987.
[26] ——, *System Identification Toolbox for use with Matlab: User's Guide Version 6*. Natick, Mass.: MathWorks, Inc., 2004.
[27] J. Löewis, "Flachheitsbasierte Trajektorienfolgeregelung elektromechanischer Systeme," Ph.D. dissertation, Fakultät Elektrotechnik und Informationstechnik, TU-Dresden, 2002.

[28] J. Löewis and J. Rudolph, "Real-time trajectory generation for flat systems with constraints," in *Nonlinear and Adaptive Control*, A. Zinober and D. Owens, Eds. New York, NY: Springer-Verlag, 2003, pp. 385–394.
[29] R. Mahadevan and F. I. Doyle, "On-line optimization of recombinant product in a fed-batch bioreactor," *Biotechnol. Prog.*, vol. 19, pp. 639–646, Jan. 2003.
[30] M. V. Nieuwstadt and R. M. Murray, "Real-time trajectory generation for differentially flat systems," *Int. J. Robust Nonlinear Control*, vol. 8, pp. 995–1020, Dec. 1998.
[31] K. Peterson and A. Stefanopoulou, "Extremum seeking control for soft landing of an electromechanical valve actuator," *Automatica*, vol. 40, no. 6, pp. 1063–1069, Jan. 2004.
[32] F. Pischinger and P. Kreuter, "Electromagnetically operating actuator," *US Patent 4,455,543*, Jun. 19, 1984.
[33] M. Pischinger, W. Salber, F. van der Staay, H. Baumgarten, and H. Kemper, "Benefits of the electromechanical valve train in vehicle operation," *SAE 2000-01-1223*, 2000.
[34] V. S. Rao, "Equivalent circuit of solid iron core for impact excitation problems," *Proceedings IEE*, vol. 111, no. 2, pp. 349–357, Feb. 1964.
[35] G. Schmitz, "Verfahren zur Regelung der Ankerauftreffgeschwindigkeit an einen elektromagnetischen Aktuator durch extrapolierende Abschätzung der Energieeinspeisung," *German Patent Appl. 19807875*, Feb. 25, 1998.
[36] N. L. Schmitz and D. W. Novotny, *Introductory Electromechanics*. New York, NY: The Ronald Press Company, 1965.
[37] M. J. van Nieuwstadt, "Trajectory generation for nonlinear control systems," Ph.D. dissertation, Department of Mechanical Engineering, California Institute of Technology, 1997.
[38] Y. Wang, T. Megli, M. Haghgooie, K. Peterson, and A. Stefanopoulou, "Modeling and control of electromechanical valve actuator," *SAE 2002-01-1106*, 2002.
[39] F. Woittennek, "Untersuchung flachheitsbasierter nichtlinearer Regler für magnetgelagerte Wellen," Master's thesis, Fakultät Elektrotechnik und Informationstechnik, TU-Dresden, Germany, 1999.